Universita' degli Studi di Padova

Dipartimento di Fisica e Astronomia

Corso di Laurea in Fisica

Modeling of low energy gas-wall interaction by molecular dynamics methods

Laureando

Luca Brescaccin

Relatore

Dott. Gianluigi Serianni

Co-relatore

Dott. Emanuele Sartori

Anno Accademico 2014/2015

Contents

Abstract

In non-isothermal flows of rarefied gases, such as those in Neutral Beam Injector (NBI) applications, the interaction with solid walls determines temperature and density gradients, and coefficients for momentum and energy accommodation can be used to investigate the interaction. In this work the translational and rotational energy relaxation of H_2 gas molecules in inelastic collision with a copper wall is studied, by a fully classic Molecular Dynamics (MD) approach. This approach permits to estimate the Accommodation Coefficients (AC) for hydrogen gas impinging on solid walls, needed to estimate the energy loss at walls and the gas flow in non-isothermal conditions. Moreover the angular distribution of scattered particles after the impact between gas and wall and the normal momentum transport to the wall have been studied.

Sommario

Nei flussi di gas rarefatti, come quelli presenti all'interno degl'iniettori di particelle neutre (NBI), l'interazione con le pareti determina il gradiente di temperatura e di densità, e i coefficienti di accomodamento per l'energia e per l'impulso possono essere utilizzati per investigare tale interazione. In questo lavoro viene studiato il rilassamento dell'energia di traslazione e di rotazione di molecole di H_2 attraverso collisioni anelastiche su una superficie di rame con un modello di Dinamica Molecolare (MD) classica. Questo approccio permette di stimare i Coefficienti di Accomodamento (AC) per un gas di idrogeno incidente su pareti solide, necessari per stimare la perdita di energia alla parete e per determinare il flusso in condizioni non isotermiche. Inoltre vengono studiati lo scambio di impulso perpendicolare alla parete e la distribuzione angolare delle particelle di gas a seguito dell'impatto tra gas e parete.

Chapter 1

Introduction

The construction of a nuclear fusion device for energy production is among the most ambitious projects mankind aver attempted. One of the most promising candidates for producing thermonuclear fusion is the tokamak magnetic configuration. In a tokamak, both the externally generated toroidal magnetic field and the poloidal magnetic field generated by plasma current play a fundamental role in the confinement [1]. The process that generates the toroidal current relies on the transformer effect which is the inductive coupling between the central solenoid and the toroidal plasma itself; this Ohmic Heating (OH) regime is limited in maximum current and duration, and only allows pulsed operations. Auxiliary heating systems can be used: nowadays most of experiments make use of both Neutral Beam Injection (NBI) and several variants of Radio Frequency (RF) heating. Auxiliary heating allows the access to high-confinement regimes (so called H-mode). Their use is fundamental to achieve long steady-state operations. Seeking for an early realisation of fusion energy, a road map was internationally agreed few years ago, tracked towards the future construction of a demonstration reactor. The road map identifies first the construction of a major experimental device, ITER, a magnetic confinement tokamak configuration. ITER shall demonstrate the scientific feasibility of fusion as energy source.

In this scenario, the development of high-power, high-efficiency, high-energy and high-reliability NBI systems is essential. The design of these devices, starting from their physical requirements presents challenging difficulties and open issues. This area of study constitutes the basis of this work.

This chapter introduces the importance of gas-wall interactions in NBI systems and introduces the main parameters and numerical simulations involved; In chapter 2 a complete description of model and numerical implementation adopted are treated. In section 2.1 the numerical instrument and

Figure 1.1: a 3D illustration of the ITER NBI system and its components.

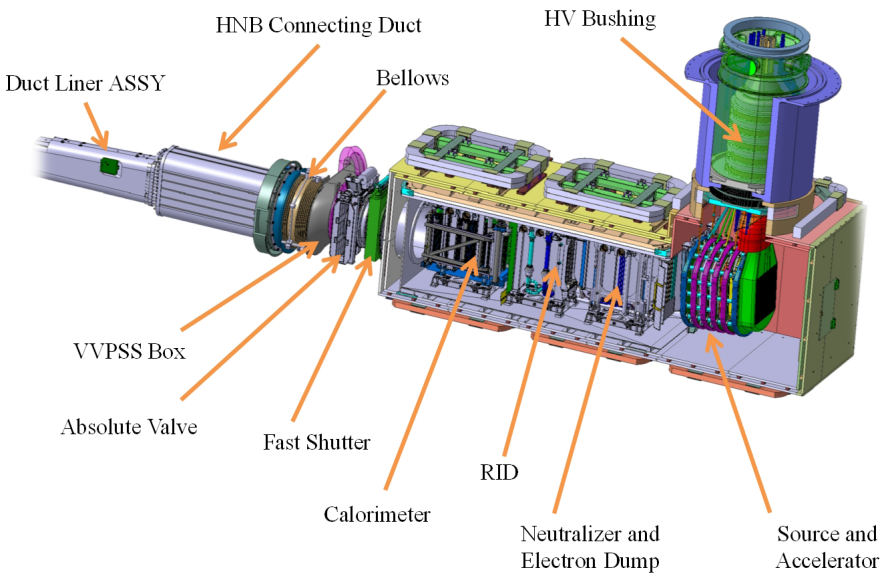

implementation are described. The gas molecule model and the wall model are treated in section 2.2 and 2.3 respectively while in section 2.4 the gas-wall interaction potential can be found. In section 2.5 the consequences of numerical implementation of the physical model are shown. In chapter 3 the the complete set of results are listed with some comparisons between different approximations.

1.1 Neutral Beam Injection system

The components of a Neutral Beam Injection (NBI) system are functional to the generation of a powerful ion beam, its neutralization, and to the transport of the neutral beam to the tokamak plasma 1.1. The Beam Source generates the ion beam: the beam passes through a Neutralizer, but some residual charges need to be stooped on a dedicated Residual Ion Dump (RID). The beam proceeds through a duct to the tokamak, but a Calorimeter to absorb its power is necessary in the case the beam shall not be coupled with the plasma.

The term Beam Source usually indicates the assembly of: the *ion source*, often plasma-based, where the ions are generated and delivered to the extraction region; the *extractor*, where an electrostatic field extract the ions and the *accelerator*, in which the ion beam is accelerated and reaches the maximum potential.

Figure 1.2: scheme of H^- accelerator in NBI system.

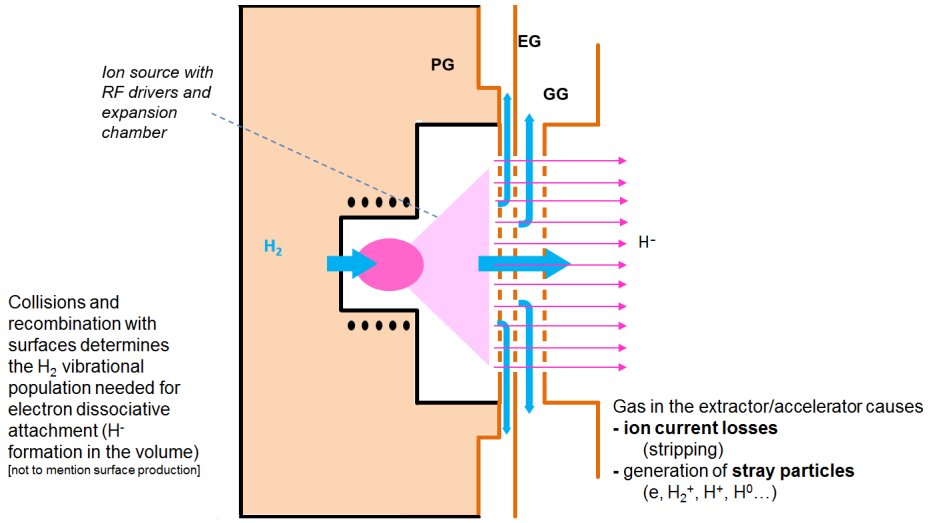

The beam negative ions are converted to neutral particles by a single-electron-detachment collision or to positive ions by double-electron-detachment collisions.

After the incomplete neutralization, the beam fraction of positive and negative ions is about 1/5 each.

In order to remove the residual charged particles there are two possible approaches , one magnetic, the other electrostatic. In the Electrostatic Residual Ions Dump (E-RID), the charged fractions are deflected by electric fields between parallel panels, capable to accept dumped power. On the other hand, a Magnetic Residual Ion Dump (M-RID) deflect the charged fractions by a magnetic field on panels located on the side of the beam; typically it is longer than E-RID and requires more space in the vacuum vessel.

1.1.1 Ion production and loss

Negative ion production involved three main processes in NBI systems: *charge transfer*, *volume production* and *surface production*. In the charge transfer mechanism alkali metals are used as electrons donors for the negative ion production. In the volume production a highly vibrational excited hydrogen molecule captures a low energy plasma electron to form a negative hydrogen ion through dissociative electron attachment process ($H_2 + e^- \rightarrow H^- + H$). In the surface production an atom emitted energetically from a low work function metal surface may leave in the form of negative ion.

Many volume destruction processes occurred in the volume are: mutual

neutralization ($H^- + H^+(H_2^+, H_3^+) \rightarrow H + ...$) electron detachment ($H^- + e^- \rightarrow H + 2e^-$) and associative detachment ($H^- + H \rightarrow H_2(\nu'') + e^-$). In the energy ranges relevant to source plasma, the sole single electron detachment collision allow few more than 1/1000 negative ions survive if the pressure is higher than 1 Pa [2].

The accelerator is generally constituted by several grids at increasing potential. The first grid (plasma grid) is involved in negative ion production thanks to the collision between neutral gas molecule impinging on it. This processes is made possible by a process involve a cesium molybdenum overlay.

The grids are also responsible of negative ion beam partial reduction. In the grids region in fact a fraction of accelerated ions is lost by processes involved background gas.

1.1.2 Ion source and accelerator condition

According to spectroscopic measurements in RF driven plasma sources for hydrogen negative ions production, the population of the first five vibrational levels of H_2 molecules in the plasma volume follows a Boltzmann distribution with T_{vib} of 5000K and up to 6000K while rotational and translational temperatures can be taken as T_{gas}=1500K [3]; gas pressure is about 1 Pa [4].

1.2 Gas-Wall interaction

In neutral beam injectors, chemical and physical processes occurring in gas-wall interaction play a fundamental role. These reactions can be at the same time necessary for beam production and detrimental for beam energy losses and for generation of stray particles that cause heat loads on components.

Gas interaction with a surface can be an inelastic or a reactive process. The inelastic reflection can be a *direct*, with reflection occurring promptly after the impact, or an *indirect* mechanism with the molecule temporarily trapped and then re-emitted from the surface. Reactive processes are dissociation of the molecule or atom recombination. In some cases the molecule can lose all its kinetic energy and remain stuck into the wall. This process is gas adsorption and can be a physical process (physisorption) or a chemical process (chemisorption).

Particle with much higher energy ($\gg$1 eV) can lead to different mechanisms such as physical sputtering. This kind of processes are not treated in this work.

1.3 Flow regimes and accommodation coefficients

Gas flow regimes are determined by Knudsen number Kn, defined as the ratio of the gas particles mean free path length and the characteristic geometrical dimension [5]. It is commonly used as an indication of the relevance of mutual gas particle collisions in a gas flow; a situation referred to as *molecular flow* occurs when the macroscopic flow behavior is mostly determined by the collisions with solid walls, and this regime is typically assumed for $Kn > 0.5$ or $Kn > 1$; free molecular flow approximation is generally considered a reasonably good approximation for the calculations related to gas flow in negative ion sources [6]. Molecular flow regime is most influenced by collision of fluid particles with wall instead of viscous effects. This issue explain the importance of the study of gas-wall interaction.

The accommodation coefficients (AC) for energy (EAC), tangential momentum (TMAC) and normal momentum (NMAC) are commonly used in models for fluids/gas flows and interaction with surfaces, especially in molecular flow regime. The accommodation coefficients are the fractions of energy/momentum transferred between the surface and the molecules. In this work the following definition of EAC will be used:

$$\alpha_E = \frac{E_i - E_r}{E_i - E_w} \tag{1.1}$$

where E_i and E_r are the average energies of incident and reflected molecules and E_w is the average energy owned by gas molecules in thermal equilibrium with the surface. It represents the fraction of energy that is exchanged with respect to the maximum possible energy exchange. It is defined on the basis of energy fluxes to the wall. The TMAC is

$$\alpha_t = \frac{mv_t - mv'_t}{mv_t} \tag{1.2}$$

where m is the molecule mass, $v_t = v\cos\theta$ is the velocity component tangential to the wall before the collision and $v'_t = v'\cos\theta'\cos\phi'$ is the velocity component of in the same direction of v_t after the collision (see figure 1.3). Finally the NMAC reads

$$\alpha_n = \frac{mv_n - mv'_n}{mv_n - p_w} \tag{1.3}$$

where v_n and v'_n are the velocity component perpendicular to the surface before and after the collision and $p_w = \sqrt{\frac{\pi}{2} m_g k_B T_w}$ with m_g gas mass and T_w temperature of wall [7].

Figure 1.3: tangential momentum exchange during collision: θ and θ' are the altitude angles, ϕ' is the azimuth angle.

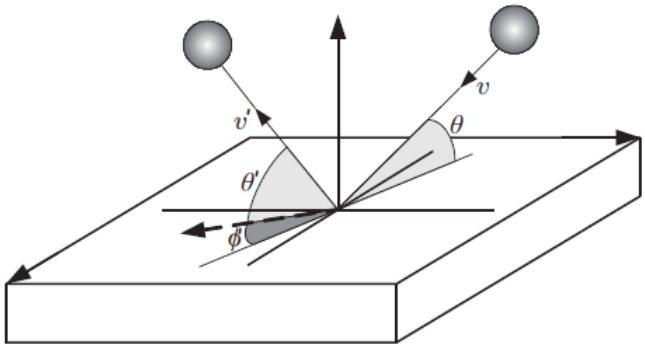

Experimental measurements to estimate α_E and α_t have been performed in the past [8]. In both cases the results have been compromised by factors like cleanness of the surfaces or irregular geometry.

1.4 Molecular dynamics

Many processes in nature can not be easily understood with mere observations: computer development and theoretical progress have partially allowed to virtually recreate systems difficult to analyze with experiments and to greatly reduce research costs. Molecular dynamics (MD) inserts itself into this picture. Specifically, it is used to replicate molecule interactions and it is profitably used in fields such as organic chemistry, protein modelling and material science.

MD simulations started with a mathematical-physical model that described the phenomenon under investigation, then differential equation involved must be discretized in order to allow computing processes. Therefore solution of the continuous equations will be approximate. The next equations show a simple example of discretization:

$$x(t) = \int_{t_0}^{t} v(\tau)d\tau \Rightarrow x(t_n) = \sum_{i=0}^{n} v(t_i)\Delta t_i \tag{1.4}$$

Many ensembles can be reproduced in MD simulation such as the microcanonical NVE, canonical NVT and isothermal-isobaric NPT ensembles. A variety of thermostat algorithms is available to add and remove energy

from the boundaries of an MD simulation in a more or less realistic way, approximating the canonical ensemble. Popular techniques to control temperature include velocity rescaling, the Nosé-Hoover thermostat, Nosé-Hoover chains [9], the Berendsen thermostat [10], the Andersen thermostat [11] and Langevin dynamics [12].

However: MD simulation could be really helpful to substitute analytical solutions of such complex problems but it might introduce cumulative errors in numerical integration. They can be minimized with proper selection of algorithms and parameters, but not eliminated entirely.

During a classical MD simulation, the most CPU intensive task is the evaluation of the potential as a function of the particles internal coordinates; for a system of N particles, calculating the force on all the particles in the system requires N(N-1)/2 calculations. A factor that increases total CPU time required for a simulation is trajectory integration and the size of the integration timestep. This is the time interval between evaluations of the potential. The timestep must be chosen small enough to balance discretization errors with work goals. Timestep and total time duration must be selected so that the calculation can finish within a reasonable time period. However, the simulations should be long enough to be relevant to the time scales of the natural processes being studied.

Potentials may be defined at many levels of physical accuracy; those most commonly used are based on molecular mechanics and embody a classical treatment of particle site-site interactions. Interaction potentials in MD are set to zero at distance higher than a chosen value, called cut-off radii, where potential influence can be neglected. In figure 1.4 a simple scheme of MD algorithm is shown.

1.5 Thesis goals

The prospective of the present thesis is to investigate the interaction between gas molecule and wall in order to improve knowledge of phenomena involved in the development of ion negative sources.

The work consists in the development of a diatomic molecule model and its implementation on numerical software that simulates low energy gas interaction with a metal lattice in classical approximation

The purpose is to obtain α_E, α_t and α_n of hydrogen H_2 impinging on copper Cu surface and the comparison with different approaches and other gas elements.

The final comparison of numerical results with data in literature is necessary in order to verify model reliability.

Figure 1.4: simplified scheme of the molecular dynamics algorithm.

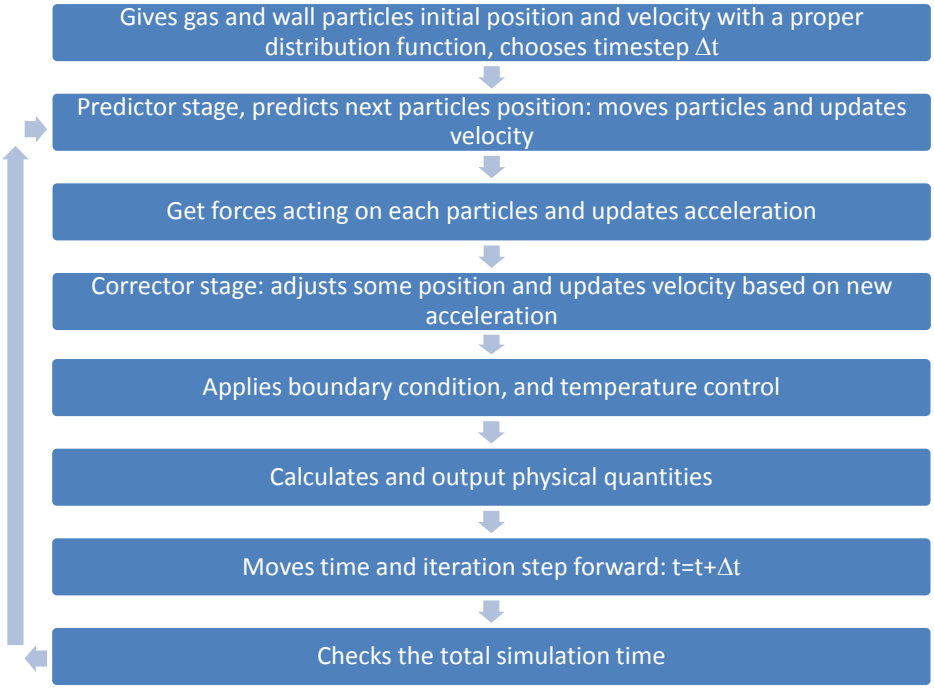

Chapter 2

Model description

The numerical model simulates the impact of a single gas particle with a slab of wall atoms. The approach consists in repeating the simulation of this collision many times, while sampling the velocity distribution related to a certain gas temperature. In this way the collision parameters that are calculated are averaged over the gas distribution function. A general description of the model and some forewords on the implementation are given in section 2.1. The gas model is described in section 2.2 while wall model is described in section 2.3. Interaction potentials are described in section 2.2 and 2.3.

2.1 MD 3D model and implementation

The interactions between elements of system are described by Morse potential [13] and by Lennard-Jones 12-6 potential [16].

The region of space in which phenomena occur is a small cubic box. The size of the box depends on the lattice parameters , but a size of about 10 Å is generally used. The wall, formed by four layers of particles ordered in lattices with typical element geometry, is placed at one side of the box and the gas particle (diatomic molecule) moves in the empty space.

The position of the gas particle center of mass is denoted with $\vec{R}_g$ and the position of a wall particle with $\vec{R}_w$.

The coordinate system is defined as follows: cartesian coordinate frame of reference is used in which the x and z axis lay on the plane of the wall surface while y axis is perpendicular and directed opposite to the wall (see figure 2.1).

Figure 2.1: representation of the system reproduced by the MD simulation program; the bottom half of the domain is occupied by wall particles and the upper part where the gas molecule moves is the region of gas-wall interaction.

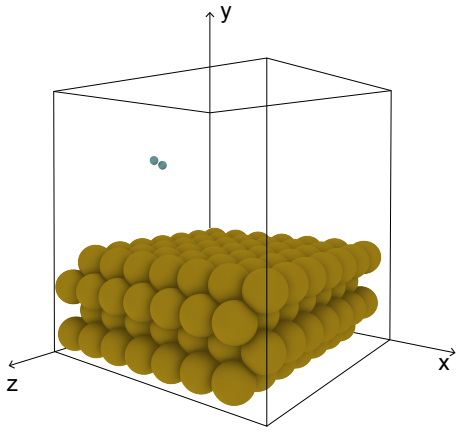

2.1.1 Particle trajectory integration

Considering a temperature of 1000K the average gas molecule velocity towards the wall is about 1000 m/s; the interaction range between gas and wall particles is about 10 Å then the duration of the gas-wall particles interaction is on average about 1 ps but it strongly depends on the vertical component of velocity v_y. A maximum simulation time of 10 ps is chosen as a good estimation of time required by the molecule to escape from the region after the collision. This abrupt interruption is needed in order to perform a large number of simulations and to collect a large statistics.

Particle trajectory is integrated using leap-frog algorithm [17]. In leap-frog integration, the equations for updating position and velocity are

$$x_i = x_{i-1} + v_{i-1/2}\,\Delta t, \tag{2.1}$$

$$a_i = F(x_i)/m, \tag{2.2}$$

$$v_{i+1/2} = v_{i-1/2} + a_i\,\Delta t, \tag{2.3}$$

where x_i is position at step i, $v_{i+1/2}$ is the velocity, or first derivative of x, at step i+1/2, m is the particle mass, a_i is the acceleration, or second derivative of x, at step i and Δt is the size of each time step.

2.1.2 Boundary conditions

Far from the surface, the gas molecule is affected by the wall, therefore it is convenient for this kind of program to set to zero the interaction potential at a suitable distance called cut-off radius of about two or three times $\sigma_{g,w}$ (see section 2.4); hence, the region of space in which the gas particle is affected by the wall potential is a small neighborhood of wall in which gas-wall interaction occurs.

It is assumed that the wall extends indefinitely, with the same properties of the modelled domain. Wall periodicity mimic an infinite repetition of the same geometry, assuming therefore that the wall surface extends indefinitely far from the surface. Analogously to the use of a cut-off radius, also the size of the wall slab can be reduced as much as possible, with a minimum size (in terms of width but also thickness) determined by the interaction sphere of the gas particles approaching the wall, and a minimum number of layers required to keep together the slab of wall particles.

With these restrictions a particle near the wall is not affected by the wall interaction that still exists outside, moreover the possibility of particle exiting the edge of the analysed region during a simulation has to be taken in account.

To solve this problem a virtual copy of cube with wall particles at the sides of the main region is recreated and the particles going beyond the edge will be moved to the opposite side of the domain (see figure 2.2).

2.1.3 Applicability of single-molecule approximation

In the macro-scale a large number of particles per second hit the wall. Each collision can be influenced by the presence of other particles.

By considering an average pressure of 1 Pa and a gas temperature (T_{gas}) of 1000K the resulting density (n) is about 10^{20} particles for cubic meter; the particles flux, calculated with $\Gamma = n\sqrt{\frac{k_B T}{2\pi m_g}}$ in which m_g is the particles mass, is in the order of 10^{23} $1/\mathrm{m}^2 s$. The portion of surface considered is about 10^{-18} m^2 and the simulation time is in the order of picosecond. The number of particles expected to approach the wall segment that is simulated is 10^4 1/s (10^{-8} 1/ps): this means that, during the 10 ps of the simulation, it is correct to assume that only one gas molecule approaches the wall and that the interaction occurs independently from other molecules.

Figure 2.2: sketch representing the need for periodic boundaries, when all the particles within the interaction radius (cut-off) must be included in the calculation of the forces; the blue point represent one gas particle and the blue circle is the region of space at distance smaller than cut-off radius. The orange particles are wall particles inside the region of interaction. The scale is not corrected.

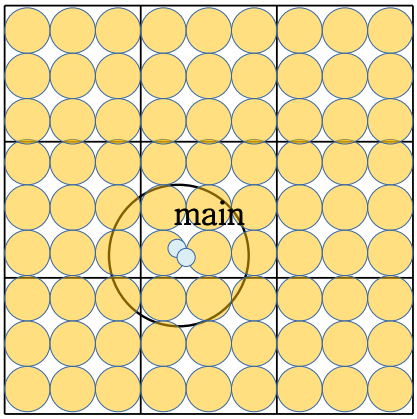

2.1.4 Numerical implementation

Program language used in this work is C++. OpenMP has been used to improve calculation speed. OpenMP (Open Multi-Processing) is an API that supports multi-platform shared memory multiprocessing programming in C, C++, and Fortran, on most processor architectures and operating systems. It consists of a set of compiler directives, library routines, and environment variables that influence run-time behavior.

In order to visualize simulation in progress openGL has been used. OpenGL (Open Graphics Library) is a cross-language, multi-platform application programming interface (API) for rendering 2D and 3D vector graphics. The API is typically used to interact with a graphics processing unit (GPU), to achieve hardware-accelerated rendering. An example of the real-time rendering will be shown in figure 3.1.

2.2 Gas molecule

Two approaches are followed for modeling the diatomic molecules: a two-site model with a fixed inter-atomic distance, and a purely classical approximation with a continuum vibrational spectrum following a Morse potential (section 2.2.1). The molecule is a system of two points $\vec{R}_1$ and $\vec{R}_2$ free to move inside the box, to rotate around its own rotation axis and to vibrate

Figure 2.3: representation of diatomic molecule reproduced by MD simulation program: the internal degree of freedom are represented, the rotation of molecule is a combination of the rotations around two different axis perpendicular to vibration axis. On the left hand side an example of oscillator can be seen and on the right hand side an example of rigid rotor with the two internal degrees of freedom.

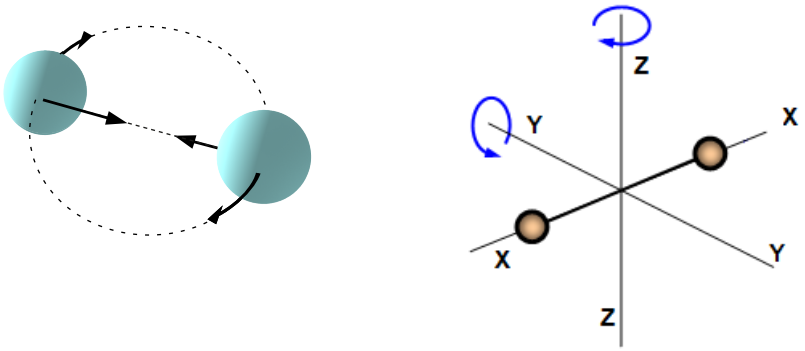

(in purely classical approximation) parallel to vector $\vec{r} = \vec{R}_2 - \vec{R}_1$. The i-th point moves in the box with velocity $\vec{v}_i = \vec{v}_{cm,i} + \vec{v}_{rot,i} + \vec{v}_{vib,i}$ in which $\vec{v}_{cm,i}$ denotes velocity of molecule center of mass, $\vec{v}_{rot,i}$ is the velocity around the rotation axis and $\vec{v}_{vib,i}$ the instantaneous vibration velocity.

In purely classical approximation the particles constituting the molecule can interact with each other and with all other particles in the system; the latter are inter-molecular interactions and are discussed in section 2.4. In the following intra-molecular interaction is discussed.

2.2.1 Intra-molecular potential

The Morse potential is a convenient inter-atomic interaction model for the potential energy of a diatomic molecule. It is a better approximation for the vibrational structure of the molecule than the quantum harmonic oscillator because it explicitly includes the effects of bond breaking, such as the existence of unbound states. It also accounts for the anharmonicity of real bonds. Morse potential is described by the following expression [13]

$$V_M(r) = D_e \left[1 - e^{-\xi\left(\frac{r}{r_0} - 1\right)} \right]^2 \tag{2.4}$$

where r is the inter-atomic distance, D_e is the dissociation energy, ξ is a parameter linked to the well width and r_0 is the equilibrium distance between

Table 2.1: constants used to model intra-molecular interaction in diatomic molecules by Morse potential.

Constants	H_2	N_2	D_2	Ref.
m $[u]$	1.007	14.007	2.016	
D_e $[eV]$	4.79	9.92	4.72	[14], [15]
ξ	1.43	2.95	1.43	[14], [15]
r_0 [Å]	0.74	1.10	0.74	[14], [15]
k $[N/m]$	567.0	2292	567.0	

atoms. The constants used to simulate diatomic molecules are listed in table (2.1).

By deriving (2.4) the force $\vec{F}_M$ acting on atoms as a function of mutual distance is obtained

$$\vec{F}_M(r) = -\frac{2D_e\xi}{r_0}\left[1 - e^{-\xi\left(\frac{r}{r_0}-1\right)}\right]e^{-\xi\left(\frac{r}{r_0}-1\right)} \cdot \frac{\vec{r}}{r} \tag{2.5}$$

A simpler model of intra-molecular interaction is the unidimensional harmonic oscillator. The potential energy and force in such a system is described by the following equations

$$V_h(r) = \frac{1}{2}k(r - r_0)^2 \qquad \vec{F}_h(r) = -k(r - r_0) \cdot \frac{\vec{r}}{r} \tag{2.6}$$

in which k is the elastic constant associate to boundary strength. Values of k and r_0 are listed in table (2.1).

The most significant difference between the two descriptions is the presence of unbound states on Morse potential. In figure 2.4 a comparison between the two potentials can be seen: with vibrational temperature $T_{vib} \leq$ 6000K (≈0.52 eV), the two curves are similar. Morse potential has been chosen for the calculation of instantaneous forces acting on the atoms mainly due to its asymmetry.

2.2.2 Initial conditions

In statistical mechanics the Maxwell-Boltzmann distribution describes particle velocity in idealized gases where the particles move freely inside a sta-

Figure 2.4: comparison between Morse and harmonic potential for H_2 molecule. The presence of non bonded states in Morse potential in the first picture can be seen. The second picture shows the similarity of two potentials for small oscillations.

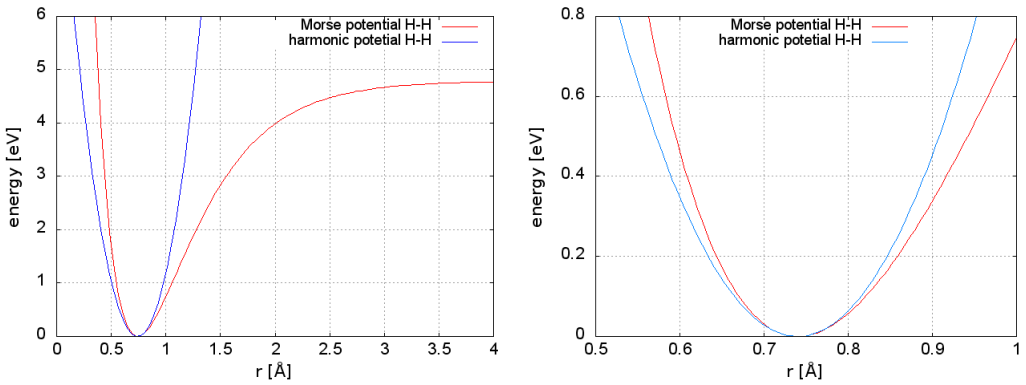

tionary container without interacting with one another, except for very brief collisions in which they exchange energy and momentum with each other or with their thermal environment. Particles in this context refers to gaseous atoms or molecules, and the system of particles is assumed to have reached thermodynamic equilibrium. The fraction of gas particles with energy E_j, mass m_g at temperature T is [18]

$$\frac{N_j}{N} = \frac{exp\left(-\frac{E_j}{k_B T}\right)}{\sum_{E_h} exp\left(-\frac{E_h}{k_B T}\right)} \tag{2.7}$$

hence upon assuming energy to be continuous and considering translation energy $E_{tras} = \frac{1}{2} m_g (v_{x,cm}^2 + v_{y,cm}^2 + v_{z,cm}^2)$ obtain

$$f_{MB}(v_{x,cm}, v_{y,cm}, v_{z,cm}) = A \exp\left(-m_g \frac{v_{x,cm}^2 + v_{y,cm}^2 + v_{z,cm}^2}{2k_B T}\right)$$

in which $A = \left(\frac{m_g}{2\pi k_b T}\right)^{3/2}$ is the normalization constant.

In Maxwell-Boltzmann theory the probability density function can be factorized by exploiting the independence of $\vec{v}_{x,cm}$, $\vec{v}_{y,cm}$ and $\vec{v}_{z,cm}$

$$f_{MB}(v_{x,cm}, v_{y,cm}, v_{z,cm}) = f_{MB}(v_{x,cm}) \cdot f_{MB}(v_{y,cm}) \cdot f_{MB}(v_{z,cm})$$

Therefore for each component the center of mass velocity can be written

$$f_{MB}(v_{i,cm}) = \sqrt{\frac{m_g}{2\pi k_B T}} \exp\left(-\frac{m_g v_{i,cm}^2}{2k_B T}\right) \tag{2.8}$$

and a gaussian normal distribution is now obtained with.

$$\sigma = \sqrt{\frac{k_B T}{m_g}} \quad \bar{v}_{i,cm} = 0 \ .$$

In this work the focus is to quantify for instance the energy exchange between gas and surfaces by considering fluxes of particles and fluxes of energies, the focus is on the representation of distribution of number of particles per unit time going towards the wall therefore, the velocity distribution of such particles directed towards the wall shall include a correction, because particles with higher perpendicular velocity v_y have a higher probability to collide per unit time; then, the perpendicular velocity v_y is sampled from

$$f(v_{y,cm}) = \frac{1}{\sigma^2} v_{y,cm} \exp\left(-\frac{v_{y,cm}^2}{2\sigma^2}\right) \ . \tag{2.9}$$

To describe the initial condition for internal energies, a similar approach can be followed. In the case of vibrational energy, two degrees of freedom have to be sampled from a distribution, namely vibration velocity $\vec{v}_{vib}$ and inter-atomic distance $\vec{r}$. Considering equation 2.7 and total vibration energy, let

$$f_{MB}(v_{vib}, r) = A \exp\left(-\frac{m_g v_{vib}^2 + k(r - r_0)^2}{2k_B T}\right) \ .$$

Magnitude of $\vec{v}_{vib}$ and $\vec{r}$ can be sampled with the following distributions

$$f_{MB}(v_{vib}) = \sqrt{\frac{m_g}{2\pi k_B T}} exp\left(-\frac{m_g v_{vib}^2}{2k_B T}\right) \tag{2.10}$$

$$f_{MB}(r) = \sqrt{\frac{k}{2\pi k_B T}} exp\left(-\frac{k(r - r_0)^2}{2k_B T}\right) \tag{2.11}$$

hence

$$\sigma_v = \sqrt{\frac{k_B T}{m_g}} \quad \bar{v}_{vib} = 0 \qquad and \qquad \sigma_r = \sqrt{\frac{k_B T}{k}} \quad \bar{r} = r_0 \ .$$

In the case of rotational energy, two further degrees of freedom are to be sampled from a distribution: angular velocity $\vec{\omega}$ is composed by two independent components $\vec{\omega}_1$ and $\vec{\omega}_2$ laying on a bi-dimensional plane orthogonal to bond direction (component along bond direction is not relevant). Magnitude of $\vec{\omega}_1$ and $\vec{\omega}_2$ can be sampled with the following distributions

$$f_{MB}(\omega_1) = \sqrt{\frac{I}{2\pi k_B T}} exp\left(-\frac{I\omega_1^2}{2k_B T}\right) \tag{2.12}$$

$$f_{MB}(\omega_2) = \sqrt{\frac{I}{2\pi k_B T}} exp\left(-\frac{I\omega_2^2}{2k_B T}\right) \tag{2.13}$$

in which $I = \mu r^2$ where r is the parameter found with the previous distribution function and $\mu = \frac{1}{4} m_g$ is the reduced mass, hence

$$\sigma_{\omega_1} = \sigma_{\omega_2} = \sqrt{\frac{k_B T}{I}} \quad \bar{\omega}_1 = \bar{\omega}_2 = 0$$

The center of mass x and z coordinates are sampled from a uniform distribution, while y coordinate (altitude) is fixed. The gas temperature T is fixed too; the velocity components $v_{i,cm}$ of center of mass are sampled using a gaussian probability density function.

$$f(x) = \frac{1}{\sigma\sqrt{2\pi}} e^{-\frac{(X-\bar{X})^2}{2\sigma^2}}$$

where $\bar{X}$ and σ^2 are respectively the expected value and variance.

In the numerical implementation, the gaussian distribution can be sampled by the box-muller algorithm [19]: a pseudo-random number sampling method for generating pairs of independent, standard, normally distributed (zero expectation, unit variance) random numbers, given a source of uniformly distributed random numbers. Suppose U_1 and U_2 are independent random variables that are uniformly distributed in the interval (0,1]. Let

$$Z_1 = \sqrt{-2\ln U_1}\cos(2\pi U_2)$$

and

$$Z_2 = \sqrt{-2\ln U_1}\sin(2\pi U_2)\ .$$

Then Z_0 and Z_1 are independent random variables with a standard normal distribution. By knowing values of σ and $\bar{X}$, two random variables normally distributed X_1 and X_2 can be obtained as $X_1 = \bar{X} + Z_1\sigma$ $X_2 = \bar{X} + Z_2\sigma$.

In case of the flux-corrected velocity distribution to sample y-component of velocity the following algorithm has been used

$$v_{y,cm} = \sqrt{-2\sigma^2 \ln(1-R)} \tag{2.14}$$

with R random number in the interval [0:1).

2.2.3 Approximations in Classical MD approach

In classical molecular dynamics, quantum-mechanics effects cannot be considered; in this paragraph the introduced approximations are discussed in the particular case of a diatomic molecule.

In quantum theory, molecular rotation energy is given by following equation

$$E_{rot,j} = \frac{\hbar^2 j(j+1)}{2I} \tag{2.15}$$

In which $\hbar$ is Planck constant divided by 2π and j is the quantum number of the angular momentum. Distance between rotational energy states is

$$\Delta E_{rot,j} = \frac{\hbar^2}{I}(j+1) \ ;$$

vibration energy levels of harmonic and Morse potential are respectively

$$E_n^h = h\nu\left(n+\frac{1}{2}\right) \qquad E_n^M = h\nu_0\left(n+\frac{1}{2}\right) - \frac{[h\nu_0(n+1/2)]^2}{4D_e} \tag{2.16}$$

and distances between energy levels for harmonic and Morse potentials are given by the following formulas respectively

$$\Delta E^h = h\nu \qquad \Delta E_n^M = h\nu_0 - \frac{h^2\nu_0^2}{2D_e}(n+1)$$

where $\nu = \frac{1}{2\pi}\sqrt{\frac{k}{\mu}}$, $\nu_0 = \frac{\xi}{2\pi r_0}\sqrt{\frac{2D_e}{\mu}}$ and n is zero or a positive integer (see table 2.2).

The vibration and rotation energy sampling with Maxwell-Boltzmann statistics is a quite strong approximation at low energies because only a discrete number of energy states are accessible to the molecule. In particular, as it can be seen in figure 2.5, which represents energy cumulative density function of vibrational and rotational energy of H_2 molecule at rotational temperature of 1500K (T_{vib}=6000K), the majority of states sampled are not accessible, the first vibrational bond state is at energy of 0.27 eV and the first rotational state is at 0.015 eV.

The accessible vibrational states at low energies are sparse, but are such that at a temperature T_{vib} of 6000K, many states are possible (say, 5) and with non negligible probability. One should notice that at 6000K a classical continuum approximation instead of the five accessible states is strong, but at least allows for energy exchange into vibrational modes. The continuum rotational energy spectrum is also a strong approximation but in the same way, the focus is on the energy exchange that is supported by a fully classical approach.

Furthermore the choice of Morse potential instead of the harmonic potential is supported by quantum considerations. In fact the first bond state for harmonic potential is twice the firs bond state of Morse potential as can be seen in table 2.2 that would lead to a stronger approximation.

Table 2.2: first rotation energy levels and first vibration energy levels in Morse and harmonic potential for H_2, N_2 and D_2.

	H_2	N_2	D_2
$E_0^h\ [eV]$	0.54	0.29	0.38
$E_0^M\ [eV]$	0.27	0.15	0.19
$E_{rot,1}\ [meV]$	15	0.49	7.6

Figure 2.5: Cumulative density function for H_2 vibration (6000K) and rotation (1500K) energy respectively. In both pictures the curves grow rapidly, energy spectrum is pressed at small values if compared with first quantum states.

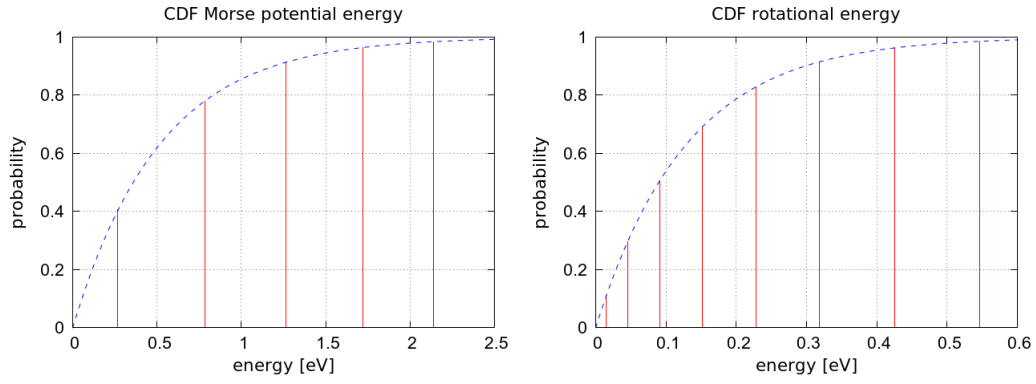

Figure 2.6: FCC unit cell geometry.

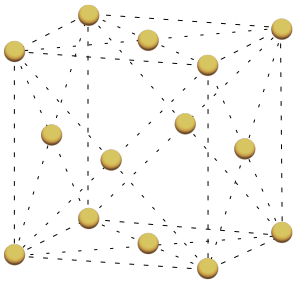

2.3 Wall

Two approaches are followed for modeling the wall: a fixed particles model and a wall with thermal agitation in which particles interact with a site-site potential. Wall temperature is maintained constant thanks to Berendsen thermostat (section 2.3.2).

For copper and platinum the unit cells are face centered cube (FCC) with edges of 392.42 pm and 361.49 pm respectively [20]. In figure 2.6 the FCC unit cell geometry is shown. The surface is obtained from the lattice cut on a (1,0,0) plane (Miller plane). The slab is typically four layers thick (1.5 unit cells). To minimize the numerical complexity, the domain is periodic (see section 2.1.2).

Position of i-th wall particle is denoted with $\vec{R}_{w,i}$.

2.3.1 Lennard-Jones potential

Since the work is focused on the gas-wall interaction and not on the modelling of the properties of the solid material, a very simple potential is chosen to model the metal wall. In this case, it is adopted a Lennard-Jones 12-6 potential, which was used in literature for the case of Cu and Pt. Interaction between i-th and j-th wall particle is described by [16]

$$V_{L-J}(r_{ij}) = 4\epsilon\left[\left(\frac{\sigma_w}{r_{ij}}\right)^{12} - \left(\frac{\sigma_w}{r_{ij}}\right)^{6}\right] \tag{2.17}$$

where $r_{ij} = \|\vec{R}_{w,j} - \vec{R}_{w,i}\|$ is the distance between the two particles, ϵ is the well depth and σ is the finite distance at which the inter-particle potential is

Table 2.3: Lennard-Jones potential parameters for Cu-Cu and Pt-Pt interaction.

	Cu-Cu	Pt-Pt	Ref.
σ_w [Å]	2.32	2.48	[21]
ϵ_w $[meV]$	167	521	[21]

Figure 2.7: comparison between Cu-Cu and Pt-Pt L-J potentials.

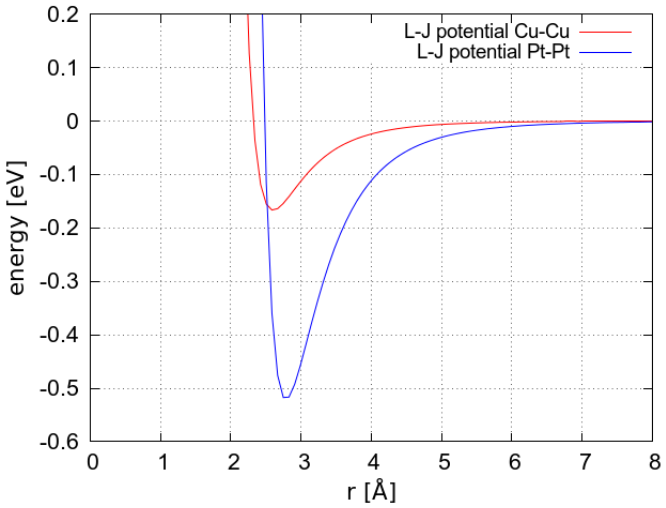

zero. Therefore, the force acting on the i-th particle is

$$\vec{F}_{L-J}(r_i) = -24\epsilon \sum_{j \neq i}^{N_{co}} \left[2\left(\frac{\sigma_w^{12}}{r_{ij}^{13}}\right) - \left(\frac{\sigma_w^{6}}{r_{ij}^{7}}\right) \right] \cdot \frac{\vec{r}_{ij}}{r_{ij}} \tag{2.18}$$

where N_{co} is the number of particles included in a sphere centered at particle i and with radius equal to the cut-off radius. In table (2.3) parameters for Cu-Cu and Pt-Pt interaction are given. The two potentials are compared in figure (2.7).

The reader should be warned that, for a more sophisticated treatment of wall particles, a model for the interaction including the electron cloud density is typically used. For instance, a potential such as the embedded-atom model (EAM) [22] is used in computational science. The EAM potential energy is a function of a sum of functions of the separation between an atom and its

neighbors. In a simulation, the potential energy of an atom, i, is given by

$$E_i = F_\alpha \left(\sum_{i \neq j} \rho_\beta(r_{ij}) \right) + \frac{1}{2} \sum_{i \neq j} \phi_{\alpha\beta}(r_{ij}),$$

where r_{ij} is the distance between atoms i and j, $\phi_{\alpha\beta}$ is a pair-wise potential function, ρ_β is the contribution to the electron charge density from atom j of type β at the location of atom i, and F is an embedding function that represents the energy required to place atom i of type α into the electron cloud.

In the original model, the latter function represents the electron density. EAM is related to the second moment approximation to tight binding theory, also known as the Finnis-Sinclair model [23]. These models are particularly appropriate for metallic systems. Embedded-atom methods are widely used in molecular dynamics simulations.

Since the electron cloud density is a summation over many atoms, usually limited by a cutoff radius, the EAM potential is a multibody potential.

The focus of this work is the gas behavior therefore the EAM potential has not been used in order to simplify the numerical issues.

2.3.2 Berendsen Thermostat

The Berendsen thermostat [10] is an algorithm to re-scale the velocities of particles in molecular dynamics simulations to control the simulation temperature.

In this scheme, the system is weakly coupled to a heat bath with a prescribed temperature. The thermostat suppresses fluctuations of the kinetic energy of the system and therefore cannot produce trajectories consistent with the canonical ensemble. The temperature of the system is corrected such that the deviation exponentially decays with some time constant τ .

$$\frac{dT}{dt} = \frac{T_0 - T}{\tau}$$

Though the thermostat does not generate a correct canonical ensemble (especially for small systems), for large systems on the order of hundreds or thousands of atoms/molecules, the approximation yields roughly correct results for most calculated properties. The scheme is widely used due to the efficiency with which it relaxes a system to some target (bath) temperature. In many instances, systems are initially equilibrated using the Berendsen scheme, while properties are calculated using the widely known Nosé-Hoover thermostat [24], which correctly generates trajectories consistent with a canonical ensemble.

Table 2.4: parameters of Lennard-Jones potential of gas-wall interaction.

Surface	$\sigma_{g,w}$ (Å)		$\epsilon_{g,w}$ (meV)	
	H/D	N	H/D	N
Cu	2.50	2.81	12.7	23.5
Pt	2.58	2.89	22.5	41.6

In the specific case of the simulation of gas-wall interaction, the thermostat is only applied to wall particles and is necessary to equilibrate the wall at the temperature required for the simulation.

2.4 Gas-wall interaction

The interaction between gas and wall particles is described by Lennard-Jones 12-6 potential (eq. 2.17). Values for $\sigma_{g,w}$ and $\epsilon_{g,w}$ are obtained from Lorentz-Berthelot rules [24]

$$\sigma_{g,w} = \frac{\sigma_g + \sigma_w}{2} \ , \qquad \epsilon_{g,w} = \sqrt{\epsilon_g \epsilon_w} \tag{2.19}$$

in which σ_g, σ_w, ϵ_g and ϵ_w are parameters of Lennard-Jones potential of gas-gas interaction and wall-wall interaction respectively. Values of $\sigma_{g,w}$ and $\epsilon_{g,w}$ are listed in table 2.4. The parameters for H-H interactions are those for site-site interaction between two H_2 molecules, taken from [25].

2.5 Model verification

As it is well known, numerical models introduce approximations in the representation of physical systems. In the following, the focus is on the effects of vibrations on the behavior of the molecular oscillator.

2.5.1 Numerical error in integrating vibration

The choice of timestep Δt is an important task for numerical model operation. The focus has to be directed towards the typical timestep of the physical model.

In the center of mass frame the equations of motion of the two atoms are

$$m_a \frac{\partial^2 \vec{r}_1}{\partial t^2} = -k(\vec{r}_1 - \vec{r}_2 + \vec{r}_0)$$

$$m_a \frac{\partial^2 \vec{r}_2}{\partial t^2} = -k(\vec{r}_2 - \vec{r}_1 - \vec{r}_0)$$

in which m_a is the mass of atoms and $\vec{r}_1$ and $\vec{r}_2$ are the instantaneous positions of the two atoms; by subtracting the first equation from the second obtain

$$\mu \frac{\partial^2 \vec{r}}{\partial t^2} = -k(\vec{r} - \vec{r}_0)$$

which is the equation of harmonic oscillator. The solution is

$$\vec{r} = \vec{r}_0 + A\cos(\omega_0 t + \phi)$$

with

$$\omega_0 = \sqrt{\frac{k}{\mu}} \ .$$

Therefore the oscillation period of H_2 molecule is

$$\tau_0 = 2\pi\sqrt{\frac{\mu}{k}} \simeq 7.63 \cdot 10^{-15} \ s \ .$$

By setting rotational energy to zero, total vibrational energy should be constant during simulations. Conversely total vibrational energy oscillates due to the finite integration time step Δt. Such oscillations can become not negligible, therefore it is necessary to estimate the oscillation amplitude as a function of the time step. There is a linear dependence of the oscillation amplitude on the integration time step as shown in figure 2.8.

According to oscillation period of H_2 molecules and according to oscillation amplitude of vibrational energy, a good compromise is taken by a Δt of 0.3 femtoseconds.

Moreover, according to the results from dedicated simulations, there is no drift with time nor increase of amplitude of this oscillation (see for instance the left picture in figure 2.8).

Translational and rotational energies are not affected by significant numerical error.

Figure 2.8: on the left is presented the vibrational energy during a simulation when rotational energy is set to zero. On the right picture show the amplitude of oscillations in function of Δt.

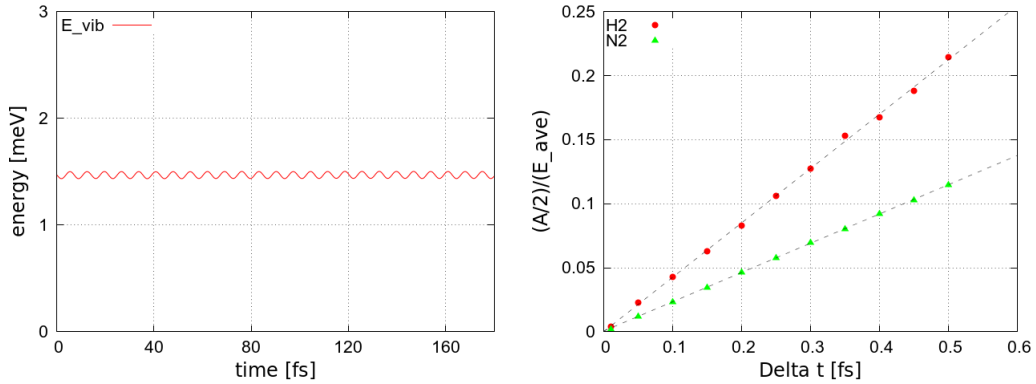

2.5.2 Rotation-vibration coupling

Additional oscillation of the internal energies will arise due to a coupling between rotational and vibrational energies. When both energies are different from zero, in the classical approximation an oscillation of rotational energy due to the variable distance of the two atoms can expected. In fact

$$E_{rot} = \frac{1}{2} I\omega^2 = \frac{1}{2}\frac{L^2}{I} \tag{2.20}$$

where L is the angular moment that is constant during one simulation since there is no external torque on the system (see figure 2.9).

It is necessary to verify that rotational energy oscillation is not due to numerical integrator. A good way to prove that is to compare the classical model expectations with numerical results. By observing figure 2.10 estimate the amplitude of rotational energy oscillations and compare it with the expected value extracted from inertia moment oscillations.

By considering the maximum and the minimum of rotational energy

$$E_{rot,max} \simeq 0.03562\ eV \quad E_{rot,min} \simeq 0.03422\ eV$$

the calculated value of ΔE_{rot} is

$$\Delta E_{rot} \approx 1.4 \cdot 10^{-3}\ eV\ .$$

The maximum and the minimum of inertia moment are

$$I_{max} \simeq 1.431 \cdot 10^{-46}\ kg\ m^2 \quad I_{min} \simeq 1.375 \cdot 10^{-46}\ kg\ m^2$$

Figure 2.9: the red line show rotational energy and the green line show vibrational energy of the molecule system. The shape of curve representing vibrational energy is changed after the introducing of rotation. The green line is the result of two perturbation with similar frequencies.

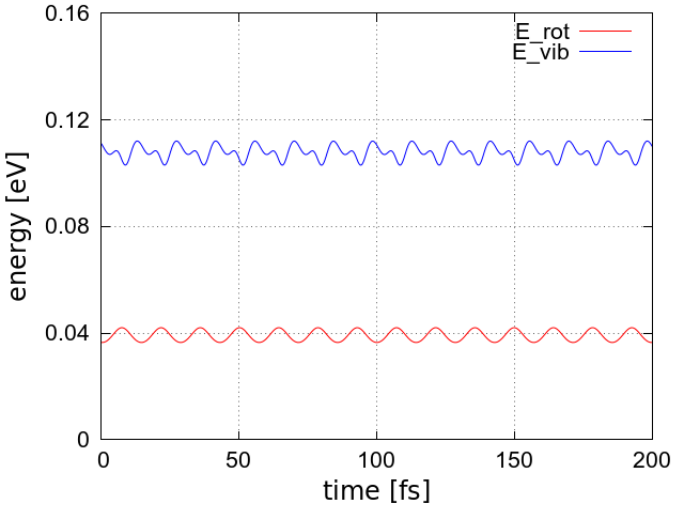

Figure 2.10: In this picture is shown the rotational energy oscillation during a simulations on the left and the inertia moment at the same time on the right.

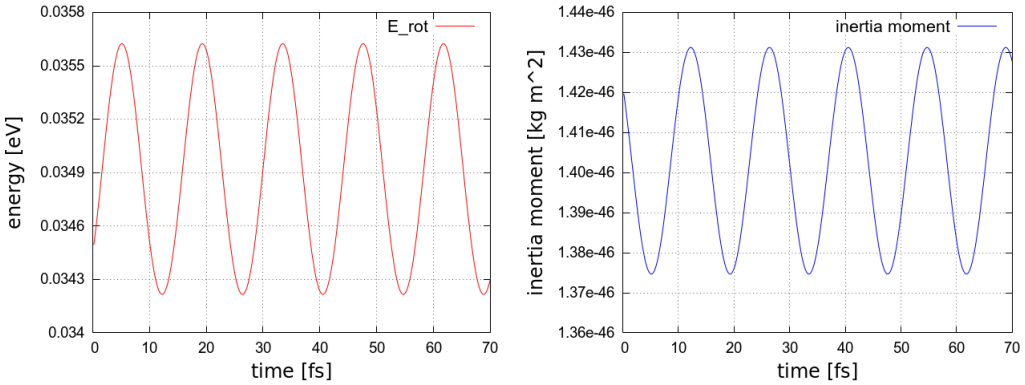

Figure 2.11: the red curve represents vibrational energy fluctuation in no-rotating molecule. By introducing rotational energy the oscillation amplitude of vibrational energy grows (blue curve). The picture on the right show the same curves after the correction.

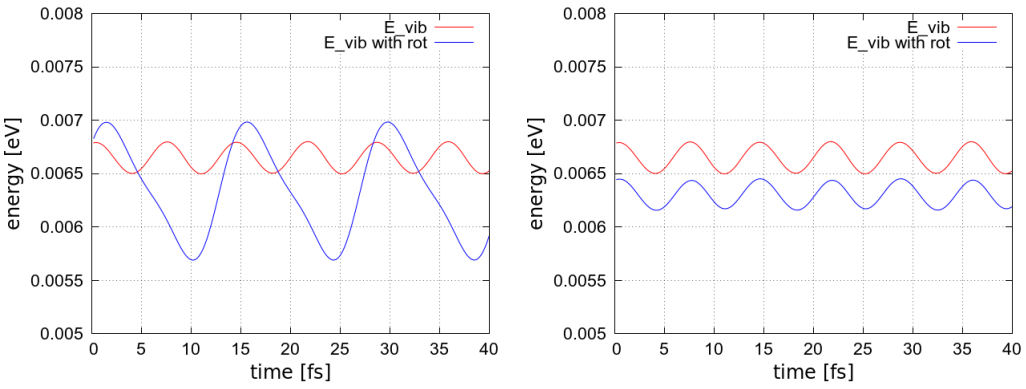

therefore using 2.20 the expected value of ΔE_{rot} is

$$\Delta E_{rot} = E_{rot,max} - E_{rot,min} = \frac{1}{2} L^2 \frac{I_{max} - I_{min}}{I_{max} I_{min}} \simeq 1,4 \cdot 10^{-3}\ eV$$

with

$$L = \sqrt{2 I_{min} E_{rot,max}} = \sqrt{2 I_{max} E_{rot,min}} \simeq 1,253 \cdot 10^{-33}\ \frac{kg\ m^2}{s}$$

The two values are compatible thus it can be assumed that rotational energy variation ΔE_{rot} is totally due to the changing distance between the two atoms in the molecule.

Another aspect shall be considered. By introducing system rotation, the fluctuation of vibration energy greatly increases its amplitude. In figure 2.11 the two lines are representative of two simulations starting with the same atomic distance and the same particle vibrational speed, determining a vibrational energy of about 6.7 meV; the oscillation of the red line is due to numerical approximation. In the case of the green line, also rotational energy is present and the shape of the oscillation changes.

The motivation has been investigated: a centrifugal force acts on the two particles due to the rotating system

$$F_c = m\omega^2 r/2 = \frac{2L^2}{mr^3}$$

that modifies total system energy. Potential energy at distance r associated to the centrifugal force is equal to the work made by external force to move

particles from distance r_0 to r

$$U_c(r) = -\int_{r_0}^{r} F_c(r)dr = \frac{L^2}{m}\left(\frac{1}{r^2} - \frac{1}{r_0^2}\right)$$

hence Morse potential including rotational effects is $V'_M = V_M + U_c$.

In figure 2.11 total vibrational energy corrected can be seen. Average values are different because, by starting at the same distance between particles ($r = 1.005\ r_0$), if the system belongs to a rotating frame of reference it will have less energy due to the presence of centrifugal force.

2.5.3 Moving averages

Given the intrinsic oscillations of vibrational and rotational energies and the presence of numerical effects, average parameters before and after the collision are needed to estimate the accommodation coefficients. Therefore it has been inserted moving average to estimate them.

As seen before the internal energies are periodic functions, thus it is necessary to choose a properly time step τ that covers at least one period. It is known that sampling values at each τ_1 (frequency ν_1), the time step of periodic function with period τ_2 (frequency ν_2), the frequency of the resulting function can be estimated as $\nu = \frac{|\nu_1 - \nu_2|}{2}$ therefore $\tau = 1/\nu$. The oscillation period of internal energies is linked to molecule vibration and sampling period correspond to integration time step $\tau_1 = \Delta t$. Estimations of vibration period for hydrogen molecule give $\tau_2 \approx 7,6 \cdot 10^{-15}\ s$. Finally a time step of 10 τ has been chosen to guarantee that enough points are taken for a satisfying average.

Chapter 3

Results and discussion

In this chapter, the accommodation coefficients and angular distributions calculated for different systems are presented. As described in the previous chapter, different approximations were used in the calculations: two approaches for the wall particles (fixed wall particles or fully atomistic wall) and two approaches for the gas molecule (rigid molecule with zero vibrational energy or Morse oscillator). In the following, these approximations are used in three combinations:

- (A rigid rotor FW) fixed wall particles (frozen wall) with fixed inter-atomic distance of gas molecule (rigid rotor),
- (B rigid rotor) fully atomistic simulation of wall particles (thermal agitation) with fixed inter-atomic distance of gas molecule,
- (C oscillator) fully atomistic simulation of wall particles with diatomic oscillator with Morse potential for inter-atomic gas interaction (fully atomistic simulation with continuous vibrational temperature).

In cases B and C the wall temperature is controlled at 300 K; in case C, we take T_{vib} = 6000 K (see section 1.1.2).

This chapter presents also different gases and wall materials. The cases of H_2-Cu is discussed in the next section and the case of deuterium in section 3.2; the interaction with a Pt surface has also been studied and results are reported in section 3.3.

3.1 H_2-Cu accommodation coefficients

Accommodation coefficients for H_2 molecule collisions with copper are shown in this section.

Figure 3.1: Image rendering of H_2-Cu simulation.

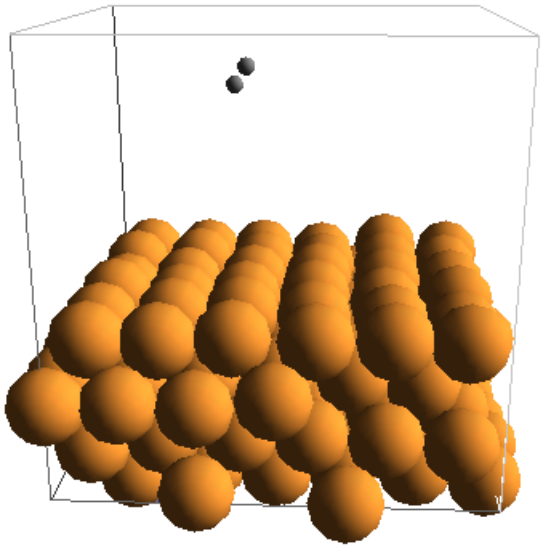

In figure 3.2, the accommodation coefficients (TMAC, NMAC and EAC) for H_2 molecule impinging on a Cu surface are shown as a function of the gas temperature T_{gas}. The dependence of corresponding angular distribution of scattered particles is shown in figure 3.3. The calculated values of TMAC, NMAC and EAC are listed in table 3.1, 3.2 and 3.3.

As expected, the calculated α_t and α_E decrease with increasing T_{gas}. The calculated α_n slightly increases with T_{gas} The three models are in good agreement. In the specific case of EAC, the vibrational energy in the estimation of the EAC is not included in order to make comparable the two approximations of molecule. In some sense, this is equal to neglecting the energy exchange that occurred in the vibrational mode for Morse oscillators.

3.1.1 Fraction of adsorbed particles

A fraction of impacting molecules is not re-emitted by the surface after the maximum simulation time that was set for computational reasons: this sticking fraction for the molecule is reported in figure 3.4. The large difference between models (B) and (C) can be explained by the very high vibrational temperature imposed in the case of the diatomic oscillator. In model (C) additional vibrational energy decrease probability of molecule attachment. In case (A) molecule do not exchange energy and normal momentum with wall, for this reason the sticky fraction is much smaller than case (B) and (C).

Figure 3.2: TMAC, NMAC and EAC for H_2-Cu system. the approximations are: (A) frozen wall with fixed inter-atomic distance (rigid rotor FW), (B) thermal wall with fixed inter-atomic distance (rigid rotor), (C) thermal wall with diatomic oscillator with Morse potential (oscillator).

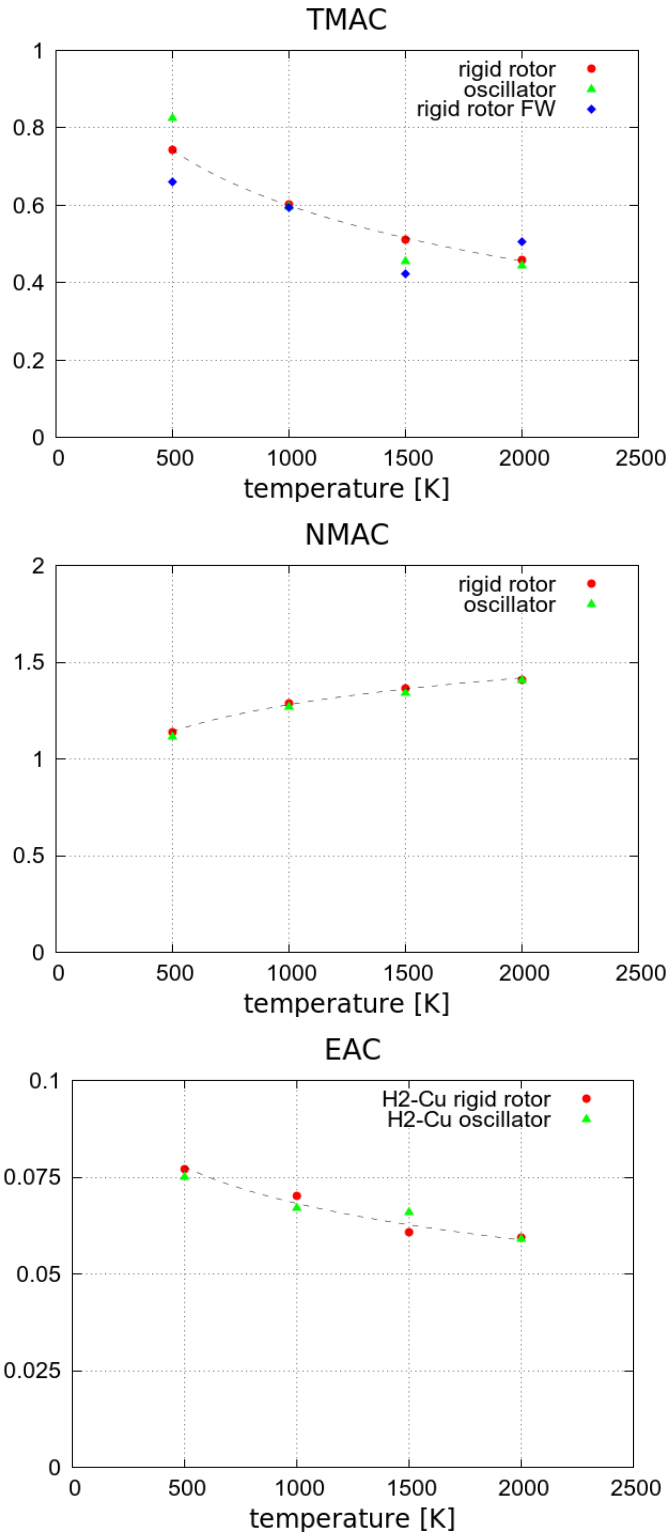

Figure 3.3: angular distribution corresponding to different TMAC values.

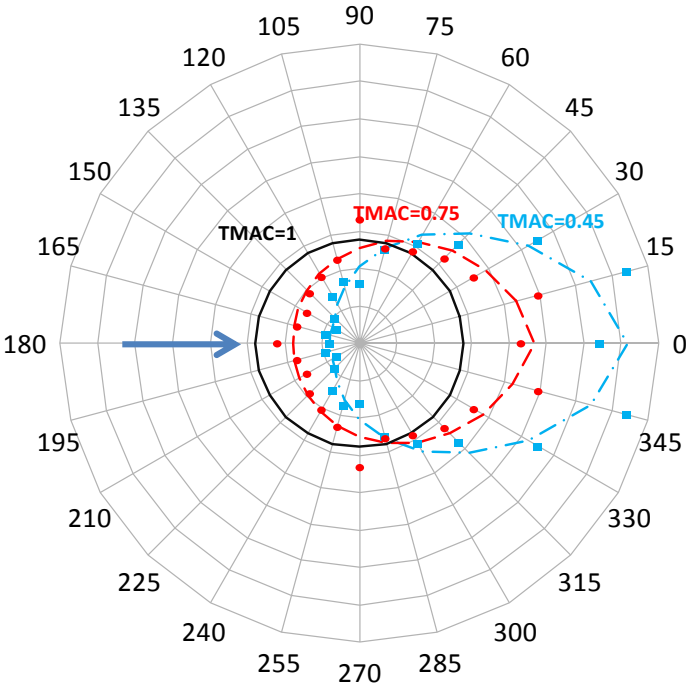

Table 3.1: TMAC for H_2-Cu system. the approximations are: (A) frozen wall with fixed inter-atomic distance, (B) thermal wall with fixed inter-atomic distance, (C) thermal wall with diatomic oscillator with Morse potential.

$T_{gas}(K)$	case A	case B	case C
500	0.660	0.743	0.826
1000	0.595	0.601	0.596
1500	0.425	0.510	0.455
2000	0.505	0.460	0.446

Table 3.2: NMAC for H_2-Cu system. the approximations are: (B) thermal wall with fixed inter-atomic distance, (C) thermal wall with diatomic oscillator with Morse potential.

$T_{gas}(K)$	case B	case C
500	1.144	1.119
1000	1.289	1.270
1500	1.366	1.344
2000	1.412	1.406

Table 3.3: EAC for H_2-Cu system. the approximations are: (B) thermal wall with fixed inter-atomic distance, (C) thermal wall with diatomic oscillator with Morse potential.

$T_{gas}(K)$	case B	case C
500	0.0771	0.0751
1000	0.0701	0.0672
1500	0.0609	0.0659
2000	0.0593	0.0592

Table 3.4: Fraction of gas molecules adsorbed by the wall for H_2-Cu system. the approximations are: (A) frozen wall with fixed inter-atomic distance, (B) thermal wall with fixed inter-atomic distance, (C) thermal wall with diatomic oscillator with Morse potential.

$T_{gas}(K)$	case A	case B	case C
500	2.1%	36.6%	11.7%
1000	1.1%	20.2%	3.7%
1500	0.8%	12.8%	2.0%
2000	0.8%	8.5%	1.3%

Figure 3.4: fraction F of molecules not re-emitted by the wall during the simulation. Maximum time duration of simulation is set to 10 ps. These molecules have been excluded from the statistic.

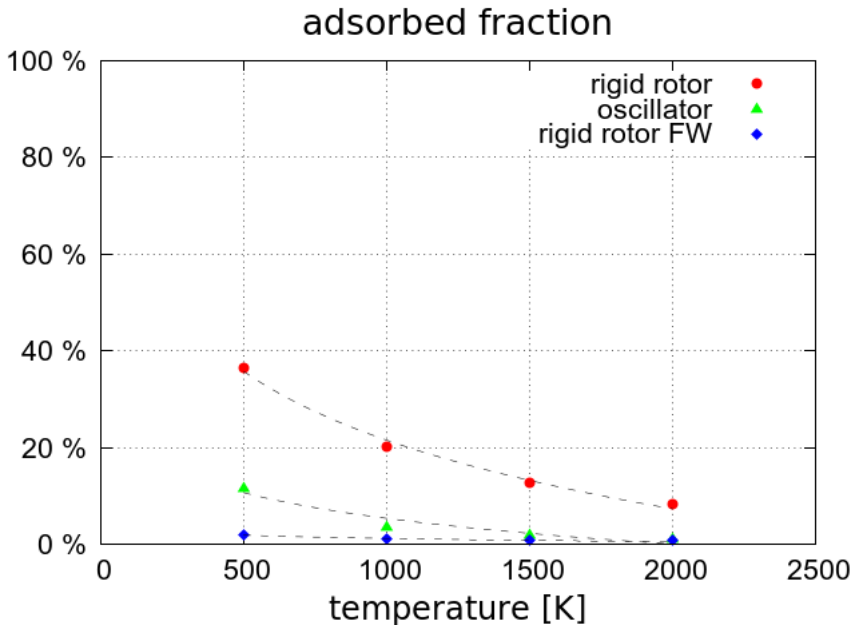

3.2 D_2-Cu accommodation coefficients

In figure 3.5, the accommodation coefficients (TMAC, NMAC and EAC) for D_2 molecule impinging on Cu surface are shown as a function of the gas temperature T_{gas} and compared with H_2-Cu system. Values of TMAC, NMAC and EAC are listed in table 3.5.

Values of α_t and α_n are in perfect agreement with H_2-Cu system. As expected values of α_E for H_2-Cu and D_2-Cu are different. In fact D_2 mass is twice H_2 mass. The Baule formula is recognized as giving a reasonable description of the effect of mass-ratio on the α_E [6]

$$\alpha_E = \frac{m_g/m_w}{(1 + m_g/m_w)^2} \tag{3.1}$$

according to the Baule formula the value of α_E for D_2-Cu is expected about twice the value for H_2-Cu.

Figure 3.5: TMAC, NMAC and EAC for D_2-Cu system compared with H_2-Cu system. The approximation used is thermal wall with fixed inter-atomic distance.

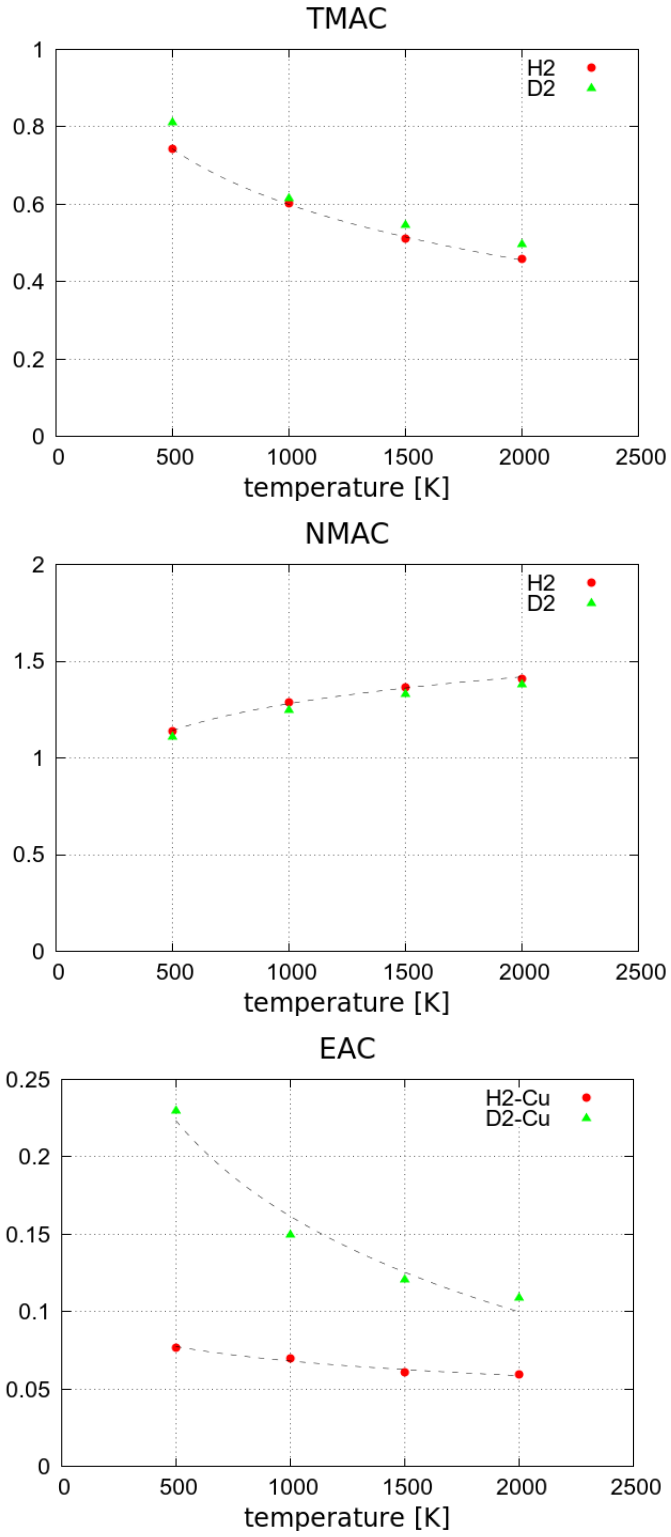

Table 3.5: TMAC, NMAC, EAC and sticky fraction F of D_2-Cu system. The approximation used is fully atomistic wall with fixed inter-atomic distance between atoms of gas molecules.

$T_{gas}(K)$	TMAC	NMAC	EAC	F
500	0.812	1.111	0.230	44.6%
1000	0.615	1.249	0.150	25.4%
1500	0.548	1.333	0.121	17.9%
2000	0.498	1.384	0.109	12.9%

3.3 H_2-Pt accommodation coefficients

In figure 3.6, the accommodation coefficients (TMAC, NMAC and EAC) for H_2 molecule impinging on a Pt surface are shown as a function of the gas temperature T_{gas} and compared with H_2-Cu system. The calculated values of TMAC, NMAC and EAC are listed in table 3.6.

While the values of α_n are quite similar, the accommodation of the tangential momentum is higher because of the stronger interaction energy used for the H_2-Pt interaction and larger mass of Pt with respect to Cu. The calculated values of α_E for H_2-Pt system at temperature of 500K and 1000K have not been considered because the number of simulations is not large enough to reduce the numerical error caused by a small energy exchange between molecule and surface.

According to Baule formula the expected α_E value of H_2-Pt system is three times smaller than the expected value of H_2-Cu system. In this sense the results are satisfying.

Figure 3.6: TMAC, NMAC and EAC for H_2-Pt system compared with H_2-Cu system. The approximation used is thermal wall with fixed inter-atomic distance.

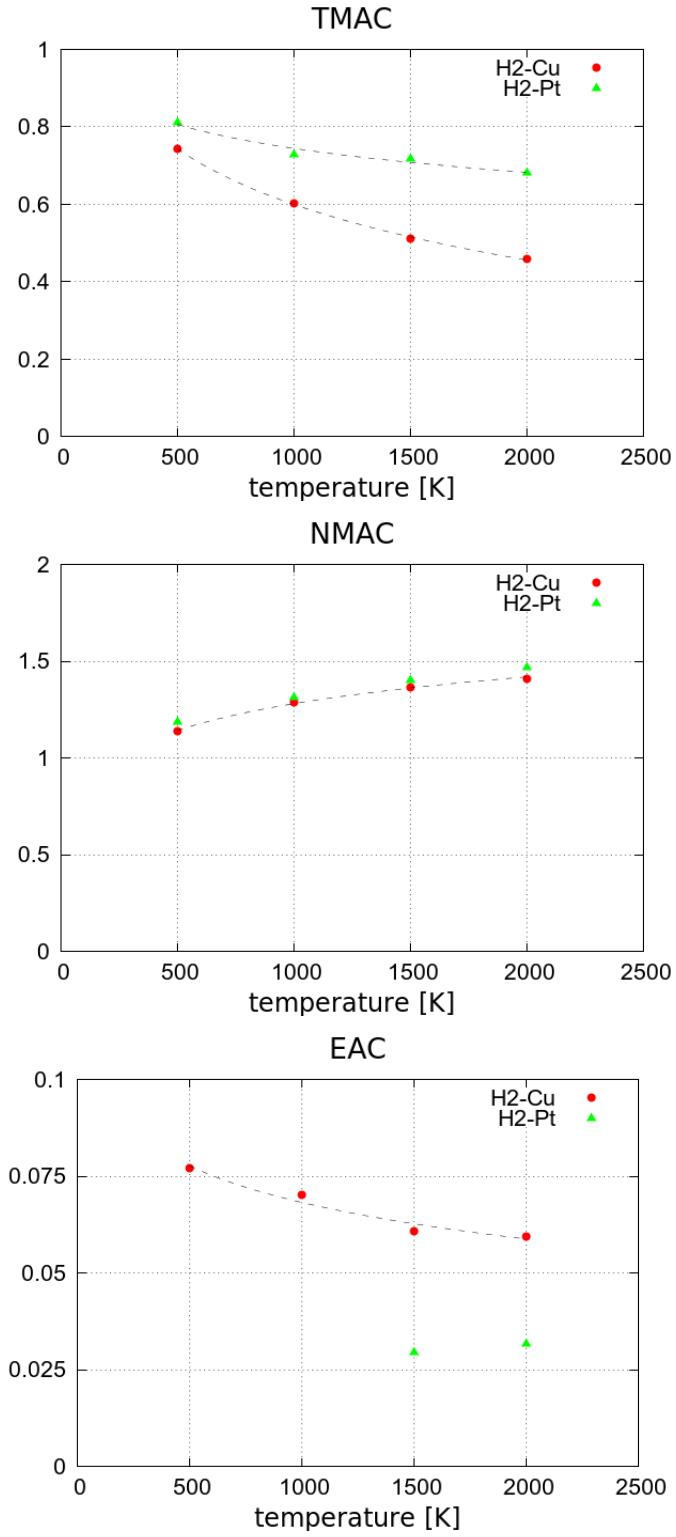

Table 3.6: TMAC, NMAC, EAC and sticky fraction of H_2-Pt system. The approximation used is fully atomistic wall with fixed inter-atomic distance between atoms of gas molecules.

$T_{gas}(K)$	TMAC	NMAC	EAC	F
500	0.812	1.188	–	43.6%
1000	0.729	1.315	–	23%
1500	0.717	1.403	0.0296	15.9%
2000	0.683	1.468	0.0318	13.4%

Chapter 4

Conclusion

It is well known that at low pressure, the interaction with walls becomes dominant in the gas flow, compared with the interaction between gas particles: the processes that determine the molecular flow regime can be approached by different numerical simulations, each addressing a different scale of the phenomena. The gas-wall interaction was studied by simulating at nanoscale the impact of a single gas molecule on an ideal surface with MD techniques.

It is been assumed that the gas particles follow a Maxwell-Boltzmann energy distribution, the box-muller algorithm and a flux corrected Maxwell-Boltzmann distribution allowed the implementation in the numerical code. The diatomic molecule was modelled by a Morse interaction potential and by a fixed inter-atomic distance in a fully classical approach. The surface and the interaction between gas and wall particles were modelled by a Lennard-Jones 12-6 potential. For the latter the Lorentz-Berthelot mixed potential parameters were used. The temperature of the surface was controlled by a Berendsen thermostat.

The numerical error dependence from the timestep integration time has been evaluated while the coupling between rotation and vibration energy has been corrected.

In order to estimate the accommodation coefficients for energy and momentum, one thousand of simulations have been performed for each temperatures. The TMAC and the NMAC were calculated for each simulation and the final results were obtained by averaging the calculated values. The initial and the final total energy of the molecule were calculated for each simulation and the averaged values were considered to evaluate the final result of EAC.

A good estimation of EAC, TMAC and NMAC has completed the lack in literature and the data were compared with different approaches, different gas element and different surface. In particular two kinds of gasses (H_2 and D_2) and two kinds of surfaces (Cu and Pt) were compared.

4.1 Comparison with data in literature

The estimation of an EAC for surfaces with sites of adsorbed gas molecules shall consider the fraction of coverage F_c. With this approximation the EAC can be estimated as $\alpha = F_c\alpha_a + (1 - F_c)\alpha_E$ where the accommodation with adsorbed H_2 molecules α_a is 0.25 according to Baule formula [6]. By considering an half coverage of H_2 particles on the platinum wall ($F_c = 0.5$) the resulting value of EAC is $\alpha = 0.14$; the estimated coefficient is compatible with the value in literature [26].

4.2 Future developments

Future developments would have to focus on a better model of the surface that includes layers of adsorbed gas molecules. Alternatively higher maximum simulation duration can be considered with a multitude of molecules impinging on surface. Moreover a different surface element will have to be taken in account, in particular molybdenum surface with adsorbed cesium. In the next step the use of Finnis-Sinclair potential might be necessary for the surface stability.

Furthermore the initial sampling of molecule degrees of freedom will have to be upgraded with more attention to the fraction of adsorbed molecules: the solution might be to restrict the initial angular distribution of center of mass velocity.

Bibliography

[1] John Wesson, *Tokamaks*, 4th ed, International series of monograph in physics, Oxford university press, Oxford, 2011.

[2] E. Sartori, *Study, analysis, design and diagnostic of plasma and beam facing components of fusion devices*, (anno), pp. 1-14.

[3] U. Fantz et al., *Nuclear Fusion* 46 S297-306, 2006.

[4] E. Sartori, P. Agostinetti, S. Dal Bello, et al., Rev. Sci. Instr. 85, 02B308, 2014.

[5] Cussler, E. L. , *Diffusion: Mass Transfer in Fluid Systems*, Cambridge University Press, 1997.

[6] E. Sartori, G. Serianni, S. Dal Bello, *Simulation of the gas density distribution in the large vacuum system of a fusion-relevant particle accelerator at different scales*, Elsevier Vacuum, 2015, p. 2, 9

[7] Bing-Yang Cao, Jun Sun, Min Chen and Zeng-Yuan Guo, *Molecular Momentum Transport at Fluid-Solid Interfaces in MEMS/NEMS: A Review*, international journal of molecular science, 2009, 10, pp. 4660-4661.

[8] F. O. Goodman, *Thermal Accommodation Coefficient*, J. Phys. Chem., 84 (12), 1980, pp. 280-299.

[9] Nosé, S., *A unified formulation of the constant temperature molecular-dynamics methods*, Journal of Chemical Physics 81 (1), 1984, pp. 511-519.

[10] Berendsen, H. J. C.; Postma, J. P. M.; van Gunsteren, W. F.; DiNola, A.; Haak, J. R., *Molecular-Dynamics with Coupling to an External Bath. Journal of Chemical Physics* 81 (8), 1984, 3684-3690.

[11] Andersen, H. C., *Molecular dynamics simulations at constant pressure and/or temperature*, The Journal of Chemical Physics, 72 (4), 1980, p. 2384 .

[12] Schlick, Tamar, *Molecular Modeling and Simulation*, Springer, 2002, p. 480.

[13] Morse, P. M., *Diatomic molecules according to the wave mechanics II. Vibrational levels*, Phys. Rev. 34, 1929, pp. 57-64.

[14] http://www1.uprh.edu/rbaretti/MorsePotential15mar2011.htm

[15] J. D. Johnson, M. S. Shaw, and B. L. Holian *The thermodynamics of dense fluid nitrogen by molecular dynamics* The Journal of Chemical Physics, 1984, p. 1284.

[16] Lennard-Jones, J. E., *On the Determination of Molecular Fields*, Proc. R. Soc. Lond, 1924, pp. 463-477.

[17] C. K. Birdsall and A. B. Langdon, *Plasma Physics via Computer Simulations*, McGraw-Hill Book Company, 1985, p. 56.

[18] F. Mandl, *Statistical Physics*, 2nd Edition, Manchester Physics, John Wiley & Sons, 2008.

[19] G. E. P. Box and Mervin E. Muller, *A Note on the Generation of Random Normal Deviates*, The Annals of Mathematical Statistics, Vol. 29, 1958, pp. 610-611.

[20] http://www.webelements.com/

[21] F. Cleri, S. Yip, D. Wolf, S. Phillpot, Phys. Rev. Lett 79(7), 1309, 1997.

[22] Daw, Murray S.; Mike Baskes. *Embedded-atom method: Derivation and application to impurities, surfaces, and other defects in metals*, Physical Review B (American Physical Society) 29 (12), 1984, pp. 6443-6453.

[23] N. W. Ashcroft and N. D. Mermin, *Solid State Physics*, Thomson Learning, Toronto, 1976.

[24] Lorentz, H. A., *Ueber die Anwendung des Satzes vom Virial in der kinetischen Theorie der Gase*, Annalen der Physik 248 (1), 1881, pp. 127-136.

[25] J.P bouanich, *J.Quant. Spectrosc. Radiat. Transfer*, 47(4). 1992, pp. 243-250.

[26] Karl Jounsten, *Handbook Of Vacuum Technology*, wiley-vch, p. 54.